Polymer 51 (2010) 2825–2835

Contents lists available at ScienceDirect

Polymer

journal homepage: www.elsevier.com/locate/polymer

# Carboxylic acid-functionalized, core–shell polystyrene@polypyrrole microspheres as platforms for the attachment of CdS nanoparticles

Ahmed Madani [a], Belkacem Nessark [a,*], Roberta Brayner [b], Hamid Elaissari [c], Mohamed Jouini [b], Claire Mangeney [b,*], Mohamed M. Chehimi [b,*]

[a] Laboratoire d'Electrochimie et Matériaux, Département de Génie des Procédés, Faculté des Sciences de l'Ingénieur, Université Ferhat Abbas, Sétif 19000, Algeria
[b] Interfaces, Traitements, Organisation et Dynamique des Systèmes (ITODYS), Université Paris Diderot & CNRS (UMR 7086), 15 rue Jean de Baïf, 75013 Paris, France
[c] Claude Bernard University Lyon-1. LAGEP Laboratory, CPE-308G 43 Bd. 11 Novembre. 1918/69622 Villeurbanne Cedex, France

ARTICLE INFO

*Article history:*
Received 15 January 2010
Received in revised form
29 March 2010
Accepted 9 April 2010
Available online 21 April 2010

*Keywords:*
Polypyrrole
Core–shell particles
CdS nanoparticles

ABSTRACT

Polypyrrole-coated polystyrene latex particles bearing *N*-carboxyl functional groups (PS@PPyCOOH) were prepared by the in-situ copolymerization of pyrrole (Py) and the active carboxyl-functionalized pyrrole (PyCOOH) in the presence of 390 nm diameter-sized polystyrene (PS) latex particles. Uncoated PS particles were prepared by emulsion polymerization of styrene. The initial comonomer fractions (in mol%) were 25/75, 50/50, 75/25 and 100/0 for pyrrole and PyCOOH, respectively. The PS@PPyCOOH$_x$ particles, where $x$ stands for the initial molar fraction of PyCOOH ($x$ = 0, 25, 50 or 75%), were characterized in terms of particle size, surface morphology, chemical composition and electrochemical redox activity using transmission electron microscopy (TEM), X-ray photoelectron spectroscopy (XPS), FTIR, TGA and cyclic voltammetry respectively. TEM showed an increase of the latex particle diameter after coating by the conducting polymer layer, from 390 nm for uncoated PS to 430 nm for PS@PPyCOOH$_{50}$ particles, allowing an estimation of the PPyCOOH shell thickness to 20 nm. FTIR and XPS detected PyCOOH repeat units at the surface of the latex particles, indicating that this monomer had indeed copolymerized with pyrrole. The core–shell structure of the PS@PPyCOOH$_x$ particles was confirmed by etching the polystyrene core in THF, leading to the formation of hollow conducting polymer capsules. Positively charged CdS nanoparticles were electrostatically assembled onto the surface of PS@PPyCOOH$_{50}$ particles, as a function of pH. It was found that, contrarily to unfunctionalized PPy-coated latex particles, PS@PPyCOOH$_{50}$ particles could be evenly decorated with stabilized CdS nanoparticles, at pH 5.

The films of the PS@PPyCOOH@CdS-coated ITO electrodes are shown to be electroactive and electrochemically stable.



## 1. Introduction

Core@shell particles with conductive polypyrrole shells coated on inorganic [1–4] or polymeric cores [5–9] have been the subject of numerous studies since the late 1980s. Indeed, polypyrrole-coated particles have enormous scientific and technological interests pertaining to the development of visual biomedical diagnostics [1c,9e], conductive composites [3e,7a], conductive paints [5b], anticorrosion coatings [8b], stationary phase in liquid chromatography [4g], conductive pigments [3f], hypervelocity experiments with microprojectiles of polypyrrole mimicking solar dusts [6].

Among the main conductive polymers, polypyrrole, polyaniline, polythiophene and poly(ethylenedioxy thiophene), the former has perhaps the broadest potential applications due to the relative ease of its synthesis via simple beaker chemistry. In addition, polypyrrole (generic name) can be prepared in the form of reactive and functional copolymers [1c,2a,10] which is an important issue regarding the immobilization of metallic nanoparticles and other nano-objects. In this regard, Chen et al. [11] have demonstrated a one step facile and versatile synthetic route to PPy–Ag nanocomposites by chemical oxidative polymerization of pyrrole using silver nitrate as an oxidation agent in aqueous media. Henry et al. [12] suggested that $PdCl_2$ acts as an efficient oxidant for pyrrole to form PPy–Pd composites in aqueous media. As far as we are concerned, we have proposed to immobilize preformed gold nanoparticles onto amino-functionalized polypyrrole-coated PS (PS@PPyNH$_2$) microspheres [9f], and human serum albumin

* Corresponding authors. Tel.: +33 144276809; fax: +33 144276814.
*E-mail addresses:* b.nessark@yahoo.fr (B. Nessark), mangeney@univ-paris-diderot.fr (M.M. Mangeney), chehimi@univ-paris-diderot.fr (M.M. Chehimi).

0032-3861/$ – see front matter © 2010 Elsevier Ltd. All rights reserved.
doi:10.1016/j.polymer.2010.04.020

(a globular protein) onto *N*-active ester functionalized polypyrrole-coated polystyrene microspheres [9a,b,c,d,e].

These examples show the importance of controlling the interface chemistry that operates at the surface of polypyrrole in order to obtain novel, robust functional heterostructures with supported globular nano-objects.

In a continuous effort to explore the surface reactivity and applications of polypyrrole particles, we aimed at interrogating the propensity of these conductive shells from PS@PPy microspheres to bind CdS quantum dots (QDs). In this regard, it is essential to consider the electrostatic interactions that occur between the QDs and the underlying PS@PPy microspheres. The efficient strategy devised so far for binding gold nanoparticles to PS@PPyNH$_2$ [9f] can thus be adopted and tuned towards the effective immobilization of CdS QDs. The rationale for immobilizing CdS nanoparticles is that one can obtain supported fluorescents QDs and design by this way novel heterostructures with synergetic effects of conductivity (owing to polypyrrole) and optical properties imparted by CdS. Alternatively, CdS QDs could act as supported photocatalysts [13], photoinitiate polymerization reactions [14], or enhance the sensitivity of polypyrrole-based biosensors [15]. Still, it is important to control the mechanisms of CdS immobilization.

In the present work, we describe the preparation, characterization and electrochemical properties of acid-functionalized polypyrrole-coated polystyrene microspheres decorated by CdS nanoparticles (PS@PPyCOOH@CdS) (see Fig. 1). The polystyrene core, average diameter 390 nm, was prepared by emulsion polymerization of styrene and poly(*N*-vinyl pyrrolidone) was used as a steric stabilizer. The reactive conducting polymer coatings consist of copolymers of pyrrole and *N*-alkyl substituted pyrrole with *N*-carboxylic acid groups (PyCOOH) at the alkyl chain end. Various poly(Py-co-PyCOOH)-coated PS latex particles were prepared with four different comonomer feed ratios (PS@PPyCOOH$_x$; *x* being the initial fraction of PyCOOH). The core–shell particles were characterized by means of transmission electron microscopy (TEM), FTIR, X-ray photoelectron spectroscopy (XPS) and TGA. Polypyrrole hollow particles were then prepared by selective extraction of the polystyrene core. Selected batches of particles were incubated with CdS nanoparticles in order to monitor the formation of assemblies between the carrier (PS@PPyCOOH) and the supported nanoparticles. Cyclic voltammetry was used to evaluate the redox properties of the QD-decorated core/shell microspheres.

## 2. Experimental

### 2.1. Materials

Styrene (Aldrich) was purified by passing through a column of activated neutral alumina. Poly(*N*-vinylpyrrolidone), with a nominal molecular weight of 360 000, was purchased from Aldrich and used without further purification. Pyrrole (Fluka) was purified by passing through a column of activated basic alumina (Arcos) prior to use. 1-(2-cyanoethyl) pyrrole (Acros), $FeCl_3 \cdot 6H_2O$ (Aldrich), ethylene glycol (Acros), lithium perchlorate ($LiClO_4$) (Acros), thiourea (Aldrich), cadmium acetate (Fluka) and α-azoisobutyronitrile (AIBN) (Fluka) were used without further purification.

The *N*-2-carboxyethylpyrrole comonomer was synthesized as described in Ref. [2a]. All aqueous solutions were prepared with deionised water.

### 2.2. Synthesis of surface functionalized polypyrrole-coated polystyrene latex particles

Polystyrene microspheres were prepared by emulsion polymerization as reported in the literature [5c]. Prior to the oxidative copolymerization of pyrroles, the PS particles were precoated with PNVP as described in [9g]. The conductive polymer coating procedure consists in the in-situ copolymerization of pyrroles in the presence of polystyrene latex. Pyrrole and PyCOOH were premixed in 25/75 (0.059 mmol/0.177 mmol), 50:50 (0.118 mmol/0.118 mmol), 75:25 (0.177 mmol/0.059 mmol) and 100:0 (0 mmol/0.236 mmol) molar ratios. This comonomer mixture was added to a vigorously stirred solution (5 ml) containing 0.1 g dry weight of PS latex and 0.09 g of $FeCl_3 \cdot 6H_2O$. The solution was stirred at room temperature for 16 h. The resulting colloidal particles were isolated by five centrifugation/redispersion cycles and redispersed in deionised water. The composite poly(Py/PyCOOH)-coated PS particles are abbreviated as PS@PPyCOOH$_x$ where *x* stands for the initial molar fraction of PyCOOH ($x = 0$, 25, 50 or 75%). The polystyrene core was selectively extracted from PS@PPyCOOH$_x$ latex particles using THF. The solution was stirred at room temperature for 24 h and the resulting hollow capsules were isolated by five centrifugation/redispersion cycles.

### 2.3. Synthesis of CdS

CdS nanoparticles were synthesized in ethylene glycol (EG) using the *Polyol method* [16–18]. Basically, cadmium acetate and thiourea were added to an 80 ml of polyol to reach a final concentration between 0.006 and 0.6 mol l$^{-1}$. The mixture was then heated at 120 °C under vigorous stirring during 1 h.

### 2.4. Coating of PS@PPyCOOH$_x$ with CdS nanoparticles

800 μl of CdS nanoparticles in aqueous solution (60 mg ml$^{-1}$) were added to 200 μl of PS@PPy and PS@PPyCOOH$_{50}$ latex particles suspension (32 mg ml$^{-1}$) and the mixture was left to react for 16 h. The pH of the mixture was adjusted to various values (2, 4, 5, 8, and 10) by addition of HCl (for acidic solutions) and NaOH (for basic solutions). After incubation, the samples were centrifuged and washed thoroughly with distilled water in order to remove the free and/or loosely bound nanoparticles. The products were characterized by TEM and XPS. It is to note that the pH set as

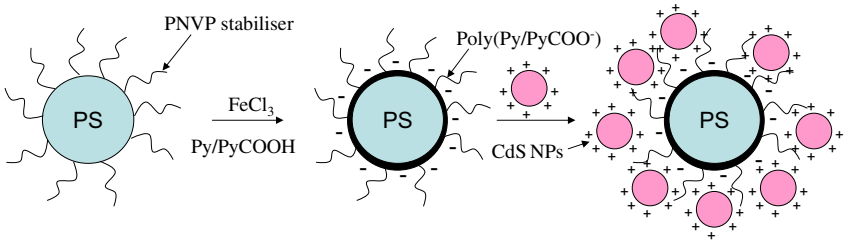


**Fig. 1.** Schematic representation of the synthesis of PPyCOOH-coated, PNVP-stabilized PS latex particles and assembly of positively charged CdS nanoparticles on the surface of negatively charged, core–shell polypyrrole-polystyrene latex particles bearing surface deprotonated *N*-ethyl carboxyl groups.

mentioned above was stable during the time scale of CdS adsorption experiments.

### 2.5. Analytical techniques

Transmission Electron Microscopy (TEM) micrographs were obtained using a JEOL JEM 100CXII UHR operating at 100 kV. Solutions containing the latex particles were cast onto Formvar-coated copper grids and the solvent was allowed to evaporate.

FTIR spectra were recorded using a Nicolet Magna 550 Series II instrument. Spectra were typically averaged over 20 scans at 4 $cm^{-1}$ resolution.

X-ray photoelectron spectroscopy (XPS) measurements were performed using a Thermo VG ESCALAB 250 instrument equipped with a monochromatic Al K$\alpha$ X-ray source (1486.6 eV). The X-ray spot size was 650 $\mu$m. The pass energy was set at 150 and 40 eV for the survey and the narrow scans, respectively. Charge compensation was achieved with a combination of electron and argon ion flood guns. The energy and emission current of the electrons were 4 eV and 0.35 mA respectively. For the argon gun, the energy and the emission current were 0 eV and 0.1 mA, respectively. The partial pressure for the argon flood gun was $2 \times 10^{-8}$ mBar. These standard conditions of charge compensation resulted in a negative but perfectly uniform static charge. Data acquisition and processing were achieved with the Avantage software, version 1.85. Spectral calibration was determined by setting the main C1s component at 285 eV. The surface composition was determined using the manufacturer's sensitivity factors. The fractional concentration of a particular element A (% A) was computed using:

$$\%A = \frac{(I_A/s_A)}{\sum(I_n/s_n)} \times 100$$

Where $I_n$ and $s_n$ are the integrated peak areas and the Scofield sensitivity factors corrected for the analyzer transmission function, respectively.

Thermogravimetric analysis (TGA) was performed on a SETARAM TGA 92-12. TGA experiments were conducted in flowing air at a ramp rate of 10 °C/min.

### 2.6. Electrochemistry

A traditional three electrodes one-compartment electrochemical cell system was used in electrochemical experiments. Glassy carbon disc (4 mm diameter) or Indium tin oxide (ITO) were used as working electrodes. Platinum grid and saturated calomel electrode (SCE) were used as counter electrode and reference electrode respectively. The cyclic voltammetry (CV) and electrochemical impedance spectroscopy (EIS) techniques were performed using EC-Lab Express V5.12 Model VSP Biologic. $LiClO_4$ (0.1 M) was used as supporting electrolyte.

## 3. Results and discussion

### 3.1. Characterization of polypyrrole-coated PS latex particles

#### 3.1.1. TEM

Fig. 2 displays TEM micrographs of PS@PPy, PS@$PPyCOOH_{25}$, PS@$PPyCOOH_{50}$ and PS@$PPyCOOH_{75}$ particles.

It is worth noting that particles are spherical with a diameter around 430 nm. The comparison between PS and PS@$PPyCOOH_x$ particles evidences significant modifications of the surface morphology following coating with the conducting polymer shell. The uncoated PS particles (TEM micrograph not shown) have a smooth, featureless surface morphology. In contrast, for

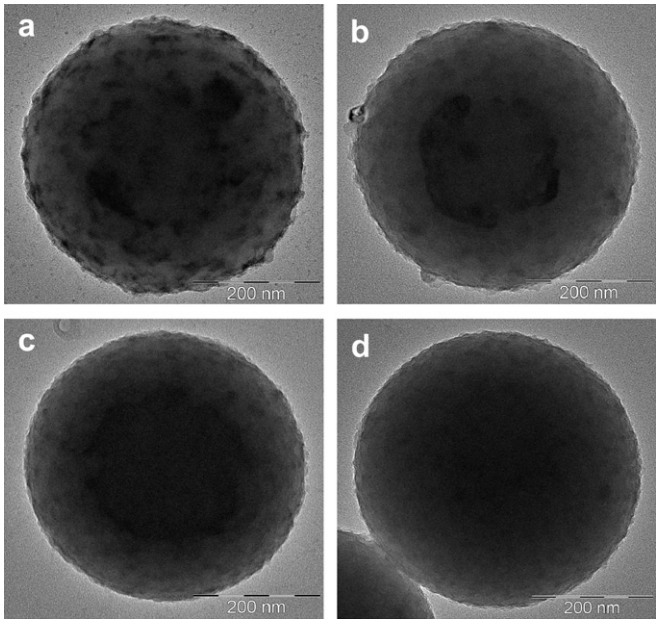


**Fig. 2.** TEM micrographs of (a) PS@PPy; (b) PS@$PPyCOOH_{25}$; (c) PS@$PPyCOOH_{50}$ and (d) PS@$PPyCOOH_{75}$ latex particles.

PS@$PPyCOOH_x$ particles, the conducting polymer overlayer induces roughening of the surface as we have observed for amine and *N*-succinimidyl ester functionalized PS@PPy microspheres [9d,e,f]. The surface roughens for higher initial pyrrole feed ratio but gets smoother when the PyCOOH fraction increases. For example, whilst PS@PPy and PS@$PPyCOOH_{25}$ particles exhibit small raised granular polymer nodules, PS@$PPyCOOH_{50}$ and PS@$PPyCOOH_{75}$ particles exhibit much smoother surfaces.

The number average diameter ($D_n$) and the polydispersity parameter ($D_v/D_n$) of particles were measured directly from the TEM images. Typically, the sizes of 50 particles were measured and the values were averaged. The $D_n$ and $D_v$ were calculated from:

$$D_n = \frac{\sum_i N_i D_i}{\sum_i N_i} \text{ and } D_v = \frac{\sum_i N_i D_i^4}{\sum_i N_i D_i^3}$$

where $D_i$ means the diameters of individual particles and $N_i$ refers to the number of particles corresponding to the diameters. As shown in Table 1, the number average particle diameter increases from *ca.* 390 nm ($D_v/D_n = 1.008$) for PS particles to *ca.* 430 nm ($D_v/D_n = 1.009$) for PS@$PPyCOOH_{50}$ particles. The difference between the diameters of the uncoated PS particles and the conducting polymer-coated PS particles gives an estimation of the conductive overlayer thickness. The $PPyCOOH_x$ thickness decreases with increasing initial PyCOOH comonomer feed ratio. This trend is most probably due to the steric hindrance brought by the carboxyl acid-terminated pendent alkyl chain end of the PyCOOH comonomer,

**Table 1**
Properties of PNVP-stabilized PS, PS@PPy and PS@$PPyCOOH_x$ latex particles.

| Samples | Diameter (nm) | Polydispersity index | Shell thickness (nm) | PPy mass loading wt.% |
|---|---|---|---|---|
| PS | 390 | 1.008 | – | – |
| PS@PPy | 460 | 1.009 | 35 | 49.0 |
| PS@$PPyCOOH_{25}$ | 440 | 1.010 | 25 | 39.5 |
| PS@$PPyCOOH_{50}$ | 430 | 1.009 | 20 | 33.8 |
| PS@$PPyCOOH_{75}$ | 410 | 1.010 | 10 | 19.5 |

which hampers the polymerization process. As a matter of fact, attempts to prepare the homoPPyCOOH shell were unsuccessful.

From the thickness of the polypyrrole overlayer and its corresponding volume, and assuming an average density of 1.5 for the conjugated polymer [2c,19] it is possible to estimate the mass loading of polypyrrole.

For PS core, the density is assumed to be 1 and for the various polypyrrole-coated PS particles the mass loading of polypyrrole was computed using:

$$\text{Wt\%} = \frac{\text{mass PPy per particle}}{(\text{mass PPy} + \text{mass PS})\text{per particle}} \times 100$$

The mass loading values are reported in Table 1.

In the specific case of PS@PPyCOOH$_{50}$ microspheres, TGA was used to assess the experimental mass loading of the conjugated polymer overlayer. Fig. 3 shows the mass loss expressed as a percentage mass of PS@PPyCOOH$_{50}$ versus temperature. The thermogram displays two regions: the first one corresponds to the calcination of polystyrene (wt. loss = 72.45% at $T$ = 354 °C); and the second region corresponds to the calcination of PPyCOOH (27.55 wt.% at $T$ = 520 °C). The experimental polypyrrole mass loading is in fair agreement with that calculated from TEM and reported in Table 1.

In order to check whether PS@PPyCOOH$_x$ particles are indeed of the core–shell type, hollow PPyCOOH$_x$ microcapsules were prepared by extracting the polystyrene core in THF. TEM micrographs of hollow PPyCOOH$_x$ (Void@PPy and Void@PPyCOOH$_{50}$) are shown in Fig. 4, indicating significant differences in the structures of the shells after selective extraction of PS core. Indeed, unbroken Void@PPyCOOH$_{50}$ particles were formed from PS@PPyCOOH$_{50}$ (this is similar to the case of PS@PPyCOOH$_{75}$) while PS@PPy (and PS@PPyCOOH$_{25}$, not shown) led to broken Void@PPy hollow particles. There are two possible explanations for the formation of these broken capsules: (i) THF could permeate the continuous PPy overlayer, causing the PS core to swell with a result of fractured polypyrrole overlayer; (ii) the polypyrrole overlayer is not completely continuous and the THF diffuses into the latex core through a patchy polypyrrole overlayer.

For high initial fraction of PyCOOH, it is possible that the continuous shells are porous so that they permit selective extraction of PS, but are robust despite a lower thickness (10 and 20 nm, see Table 1). It is possible that hydrogen bonding between adjacent COOH groups impart improved mechanical resistance to PPyCOOH$_{75}$ and PPyCOOH$_{50}$ shells compared to the more brittle PPy and PPyCOOH$_{25}$ capsules.

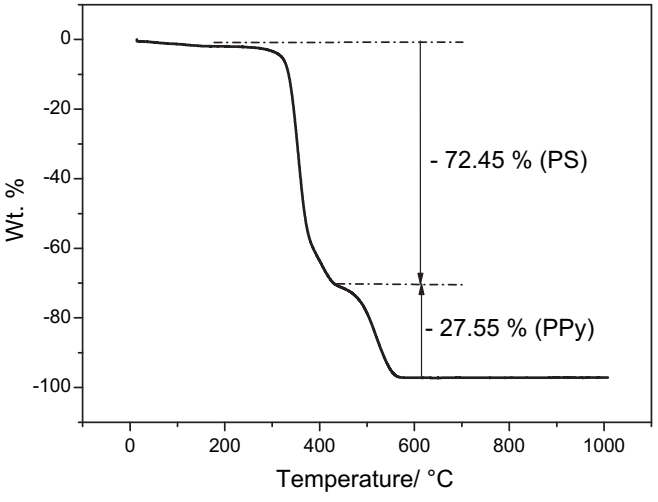


**Fig. 3.** TGA thermogram of PS@PPyCOOH$_{50}$ microspheres.

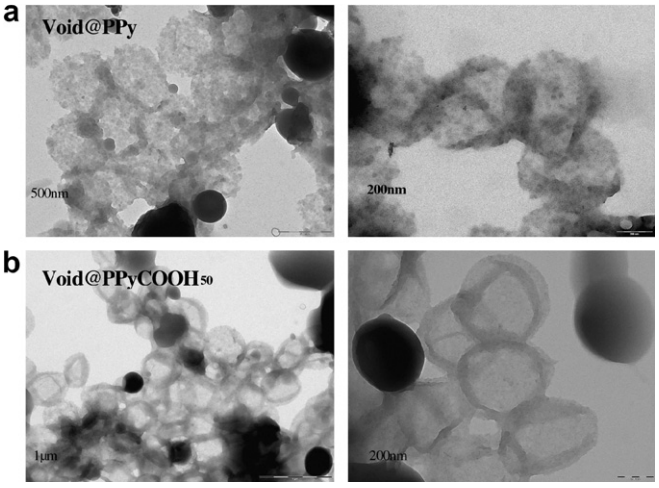


**Fig. 4.** TEM micrographs of Void@PPy and Void@PPyCOOH$_{50}$ hollow capsules obtained by polystyrene core etching in THF.

### 3.1.2. FTIR

FTIR spectra, in the 2000–1000 cm$^{-1}$ region, of PS and PS@PPyCOOH$_{75}$ particles are shown in Fig. 5. The spectra account for the expected structure of the materials since peaks due to polystyrene (especially at 1453 and 1494 cm$^{-1}$) are observed for both PS and PS@PPyCOOH$_x$, while additional bands due to the conducting polymer shell are observed for PS@PPyCOOH$_x$ only. One can note among others one band at 1560 cm$^{-1}$ due to the polypyrrole conjugated chain and one band at 1685 cm$^{-1}$, characteristic of the carboxyl groups. The steric stabilizer P*N*VP is also detected (at 1605 cm$^{-1}$) showing that it remains adsorbed on the PS surface even after coating by the conducting polymer layer. The intensity ratio of the band at 1685 cm$^{-1}$ (due to the carboxyl groups) to the bands at 1453 and 1494 cm$^{-1}$ (characteristics of polystyrene) has been plotted as a function of the PyCOOH comonomer fraction in the synthesis medium (see Inset in Fig. 5). It is clear, from this plot, that the intensity of the peak at 1685 cm$^{-1}$ increases monotonically with the initial fraction of PyCOOH. Therefore, there is a progressive incorporation of the PyCOOH comonomer in the copolymer shell with increasing initial fraction.

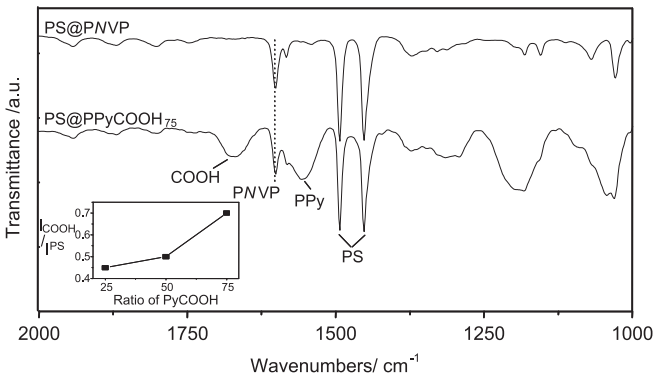


**Fig. 5.** FTIR spectra of PS and PS@PPyCOOH$_{75}$ latex particles in the 1000–2000 cm$^{-1}$ region. Inset shows the intensity ratio $I_{COOH}/I_{PS}$ of the carboxyl band (at 1685 cm$^{-1}$) to the PS bands (at 1494 and 1453 cm$^{-1}$) plotted against the PyCOOH fraction in the synthesis medium.

*3.1.3. XPS*

Fig. 6 displays survey spectra of P*N*VP-stabilized PS, PS@PPy and PS@PPyCOOH$_{75}$ latex particles. The main peaks are C1s, N1s and O1s centered at 285, 400 and 532 eV, respectively. It is noteworthy that N1s and O1s relative peak intensities are fairly high by comparison to the same peaks from the underlying P*N*VP-stabilized PS due to the contribution of the polypyrrole shells, i.e. nitrogen from the backbone and oxygen from the pendant COOH groups.

Inset of Fig. 6 displays the minor Cl2p peak (198 eV) regions for PS@PPy, PS@PPyCOOH$_{25}$ and PS@PPyCOOH$_{75}$. Interestingly, for an initial PyCOOH feed ratio as low as 25%, the Cl2p gets very noisy with quasi absence of chlorides from the PPyCOOH$_{25}$ shell. The effect is exacerbated in the case of PS@PPyCOOH$_{75}$. This most probably indicates that PPyCOOHx copolymer shells are co-doped by both chlorides and carboxylates. For a PyCOOH feed ratio higher than 25%, the conductive copolymer shell is "auto-doped" at a very high extent since chlorides are not detected by XPS. Elsewhere, for pure PPyCOOH films and powders, Lee et al. [20] reported 12.8 and 4.9% doping by chlorides (Cl/N ratio), respectively. However, these XPS results were not supported by any Cl2p or survey spectra. Although they attributed such a low doping to conductivity, nevertheless it is likely that the carboxylates act as co-dopants. This auto-doping by carboxylates might result in low conductivity for PS@PPyCOOH compared to PS@PPy since PPyCOOH is about 4 orders of magnitude less conductive than pure polypyrrole(Table 2).

The approach reported for the analysis of PMMA-coated PPy powders was used to determine the relative proportion of P*N*VP on the uncoated PS latex [21]. One can assume that:

$$C_{PS\text{-}PNVP} \approx C_{PS} + C_{PNVP}$$

where $C_{PSL}$, $C_{PS}$, and $C_{PNVP}$ are the atom % of carbon for P*N*VP-stabilized PS latex, PS latex and P*N*VP, respectively. According to the chemical formula of P*N*VP:

$$C_{PNVP} = 6\ N_{PNVP}$$

where $N_{PNVP}$ is the atom % of N due to the P*N*VP component in the PS latex. It follows that $C_{PNVP} \approx 20\%$ and $C_{PS} \approx 72\%$. P*N*VP and PS repeat units contain six and eight carbon atoms, respectively. Thus, the relative proportion of P*N*VP at the PS latex surface is

$$\%\ PNVP = (20/6)/[(20/6) + (72/8)] = 27\%$$

**Table 2**
Reports the apparent surface chemical composition of P*N*VP-stabilized PS, PS@PPy and PS@PPyCOOH$_x$ latex particles.

| Samples | C | N | O | Cl | O/C |
|---|---|---|---|---|---|
| PS@PNVP | 92 | 3 | 5 | | 0.05 |
| PS@PPy | 80.52 | 11.6 | 6.54 | 1.35 | 0.081 |
| PS@PPyCOOH$_{25}$ | 80.95 | 10.54 | 8.36 | 0.16 | 0.103 |
| PS@PPyCOOH$_{50}$ | 78.3 | 10.12 | 11.6 | 0 | 0.15 |
| PS@PPyCOOH$_{75}$ | 78 | 9.54 | 12.5 | 0 | 0.16 |

This relative proportion of P*N*VP at the surface of the latex particles is the same as the value obtained by Lascelles and Armes [5c,22] for their 1.6 μm PS latex, synthesized by dispersion polymerization. One observes an increase in the O1s/C1s peak intensity ratio as the PyCOOH repeat units are incorporated in the conducting copolymer shell. In comparison to PS@PPy, the oxygen fractions are almost two times higher for PS@PPyCOOH$_{75}$ which testifies for the presence PyCOOH repeat units at the surface of the conductive microspheres. XPS is a surface-sensitive technique with a typical analysis depth of 10 nm (in the case of organic coatings), which is markedly lower than the 25–50 nm thick conducting polymer shell as determined by TEM. Provided the conducting shell covers uniformly the PS core, the XP spectra should reflect only the conducting polymer layer. However, the experimental surface atomic percents for PS@PPy are quite far from the theoretical structural formula of PPy. The experimental N1s atomic fraction is much lower for PS@PPy (11.6%) than expected for pure PPy ($N = 20\%$). This can be explained by the detection of the underlying PS core with high carbon and low nitrogen content, suggesting that the PPy overlayers are somewhat "patchy". This is in agreement with the results obtained by the extraction experiments which showed a porous and nonuniform PPy shell. On the other hand, while the fraction of PyCOOH comonomer increases in the copolymer, the experimental surface atomic percents resemble more and more that of pure PPyCOOH$_x$. For instance, for PS@PPyCOOH$_{75}$, the experimental carbon (78%), nitrogen (9.5%) and oxygen (12.5%) atomic percents fit well with the expected theoretical values, i.e. 74% for carbon, 10% for nitrogen and 16% for oxygen. This provides further evidence that these particles possess "core–shell" morphology with a regular and uniform conducting polymer coating, as previously demonstrated by the PS core extraction experiments.

The incorporation of PyCOOH repeat units in the conjugated copolymer overlayer can be related to the bulk composition

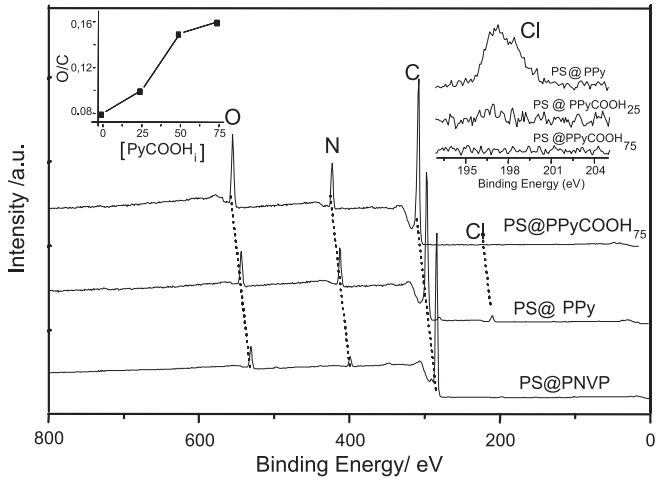


**Fig. 6.** XPS survey scans of uncoated PS, PS@PPy and PS@PPyCOOH$_{75}$ latex particles. Insets show plot of O/C surface atomic ratio versus the initial % of PyCOOH, and high resolution Cl2p regions.

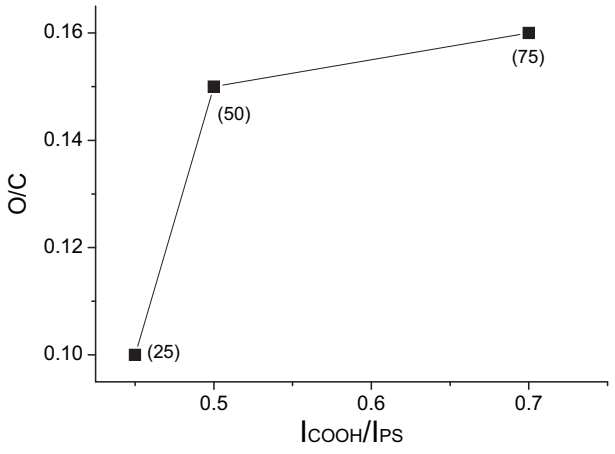


**Fig. 7.** Plot of XPS-determined O/C surface atomic ratio versus the IR-determined $I_{COOH}/I_{PS}$ intensity ratio for PS@PPyCOOH$_x$ microspheres. The initial molar fraction (in %) of PyCOOH is indicated between brackets.

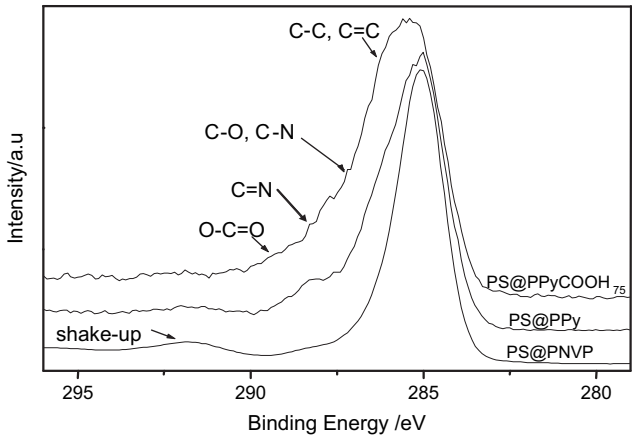


**Fig. 8.** High resolution C1s XP spectra of uncoated PS, PS@PPy and PS@PPyCOOH$_{75}$ latex particles.

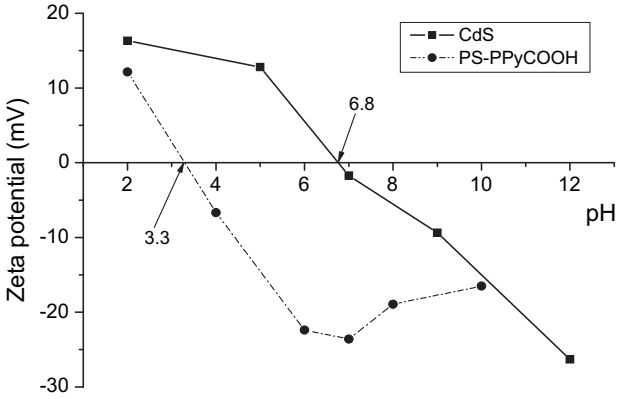


**Fig. 10.** Zeta potential of CdS nanoparticles and PS@PPyCOOH.

reflected in the IR spectra. Fig. 7 shows a plot of surface O/C ratio versus $I_{COOH}/I_{PS}$ IR peak intensity ratio (as defined in Section 3.1.2).

The high resolution C1s spectra are shown in Fig. 8 for the uncoated, PPy and PPyCOOH$_{75}$-coated PS particles. For PS, the C1s region exhibits a sharp main component centred at 285 eV (C–C, C=C) and minor components centred at 286.3 (C–N) and 288 (N–C=O). The latter two features are due to the P*N*VP stabilizer. In addition, a distinct low intensity peak at 291.7 eV is due to a π–π* "shake-up" satellite characteristic of the aromatic pendent phenyl group from styrene repeat units. For PS@PPy, the C1s region experiences a significant change resulting in the broadening of the main component centred at 285 eV, due to the introduction of C–C/C–H, C–N and C=N bonds particularly. Furthermore, the oxidation of PPy leads to an increase of the intensity of the component at 288 eV, due to C=O bonds. For PS@PPyCOOH$_{75}$ particles, the C1s region is even broader and displays a new component at 289 eV, assigned to O–C=O carboxyl groups, not observed for PS and PS@PPy particles. Moreover, the shake-up satellite, fingerprint of polystyrene, vanishes following coating by the conducting shell. This significant decrease in the proportion of the shake-up satellite actually occurs only when polypyrrole coating is uniform and quite thick [23]. For patchy polypyrrole coatings, the polystyrene shake-up satellite remains very well detected [24,25].

### 3.2. Decoration with CdS nanoparticles

Prior to the presentation and discussion of results pertaining to the decoration of PS@PPyCOOH$_x$ microspheres by CdS nanoparticles, we shall first consider some of the physicochemical properties of CdS and also the electrophoretic mobility of the former microspheres. In this section, PS@PPyCOOH particles were prepared from a comonomer mixture of 50% PyCOOH and 50% Py. This initial feed ratio was expected to provide a reasonable quantity of carboxyl acid groups at the surface of PPyCOOH$_x$ shell that is able to bind CdS dots. In addition, it will provide a shell with reasonable conductivity for further electrochemical characterization.

Fig. 9a shows the transmission electron micrograph of CdS nanoparticles. The image confirms that the CdS nanoparticles were obtained with an average diameter of about 10 nm. The lattice fringes in the micrographs indicate the crystalline nature of the particles. Fig. 9b shows the photoluminescence spectrum of CdS nanoparticles with an emission maximum at ~570 nm and full width at half maximum (FWHM) less than 30 nm, suggesting that the nanoparticles have a narrow size distribution. Note that the asymmetry of the peak in Fig. 9b is due to the photoluminescence of the polyol medium where CdS nanoparticles are suspended.

The colloidal nanoparticles are stabilized by surface positive charges due to surface defects resulting from a lack of sulphur atoms [26].

Fig. 10 shows the zeta potential of CdS nanoparticles and PS@PPyCOOH. In the pH range of 3.3–6.8, CdS nanoparticles and PS@PPyCOOH microspheres have zeta potentials with opposite signs. It is thus suspected that at this pH range CdS nanoparticles can be immobilized electrostatically on PS@PPyCOOH$_{50}$ microspheres.

Aqueous suspensions of stabilized CdS nanoparticles (10 nm-sized) were mixed with PS@PPyCOOH$_{50}$ particles for 12 h at pH 4, 5, 8 and 10. The amount of CdS nanoparticles was in slight excess of that estimated for full monolayer coverage of the latex particles

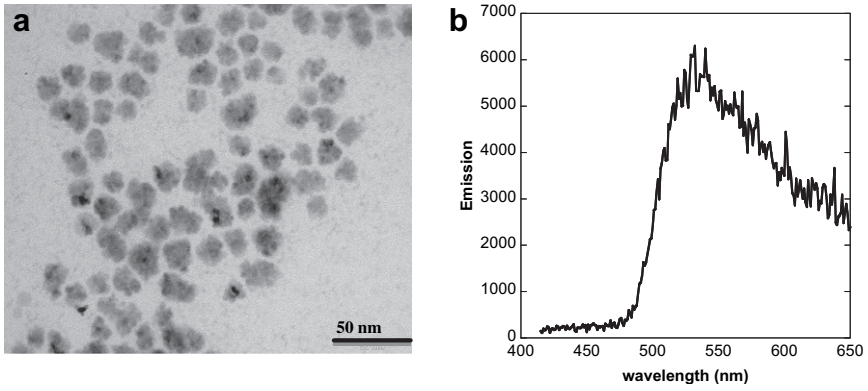


**Fig. 9.** The transmission electron micrograph of CdS (a) and the photoluminescence spectra of CdS (b).

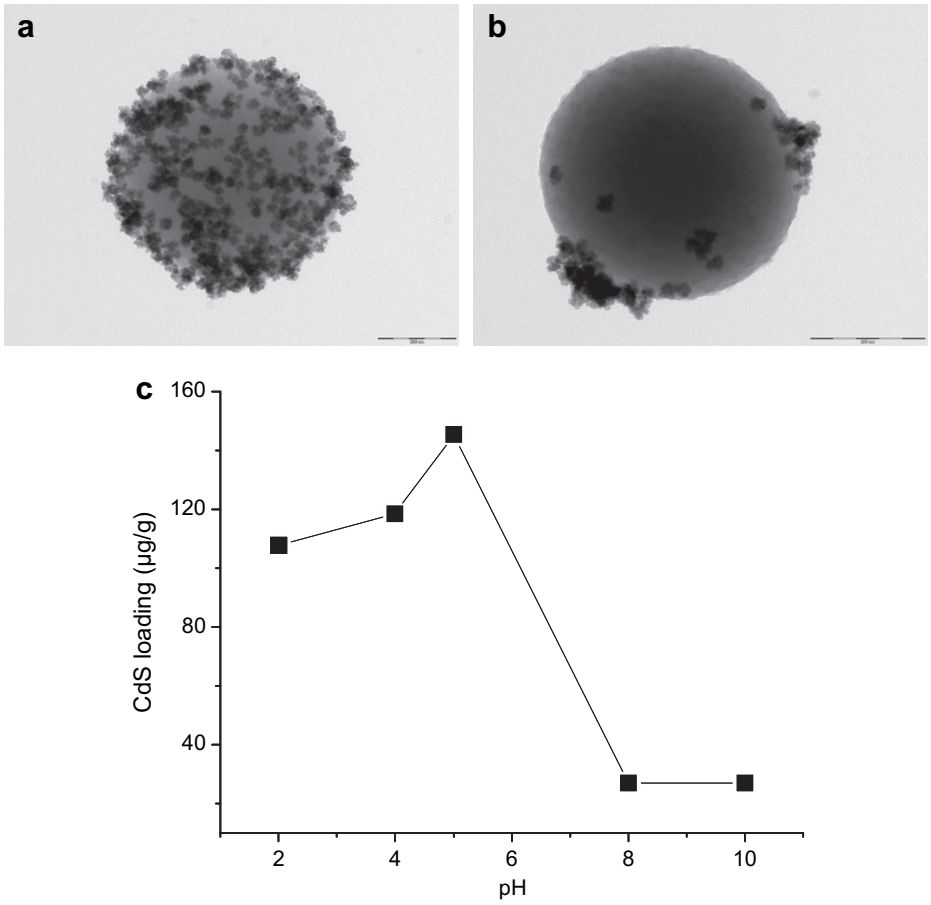


**Fig. 11.** TEM micrographs of CdS-decorated PS@PPyCOOH$_{50}$ latex particles at (a) pH 5 and (b) pH 8; and (c) CdS mass loading versus pH.

surface. The resulting core–shell particle ensembles were then precipitated, rinsed, and redispersed several times to remove loosely bound nanoparticles. Transmission electron microscopy (TEM) images of the spherical microparticle ensembles were used to investigate the morphology of the CdS-decorated PS@PPyCOOH$_{50}$ particles. Fig. 11 clearly shows that pH influences dramatically the coverage rate of the latex particle surface by CdS. Indeed, at pH 5, the latex surface appears to be fairly evenly decorated with CdS nanoparticles. While at pH 8, the microsphere surface is almost free from CdS nanoparticles.

Quantitatively, CdS mass loading on PS@PPyCOOH$_{50}$ at different pH values was estimated by counting the number of CdS nanoparticles per 1 g of PS@PPyCOOH using the *Analysis* software, and by considering a density of 4.825 for CdS. Fig. 11c shows explicitly that the optimal pH is 5, while at high pH, CdS loading is very low. In the latter situation (high pH), Fig. 10 shows that both adsorbate and adsorbent are negatively charged and thus repulsive interactions operate at the interface. In addition, there is colloidal instability of the CdS nanoparticles which are known to aggregate at pH above 7. In contrast, at acidic pH, electrostatic interactions are very favourable for the adhesion of CdS to PS@PPyCOOH$_{50}$ microspheres. Indeed, the dispersions have been subjected to repeated centrifugation/redispersion cycles, and the CdS QDs withstood separation from the underlying PS@PPyCOOH despite differences in size and mass of the microspheres and the nanoparticles. For comparison, PS@PPy particles were also incubated with CdS nanoparticles at pH 5 during 12 h and purified by several cycles of centrifugation-redispersion. TEM micrograph of the resulting latex particles is shown in Fig. 12. It is noteworthy that the PS@PPy latex particles surface is almost free from CdS nanoparticles. Since the PPy shell is

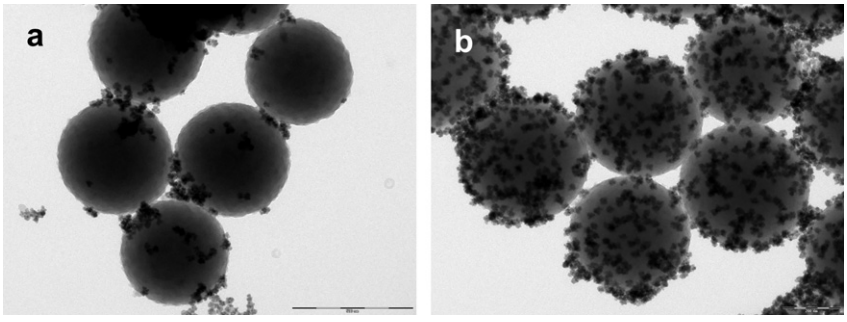


**Fig. 12.** TEM micrographs of a) CdS-decorated PS@PPy and b) CdS-decorated PS@PPyCOOH$_{50}$ latex particles at pH 5.

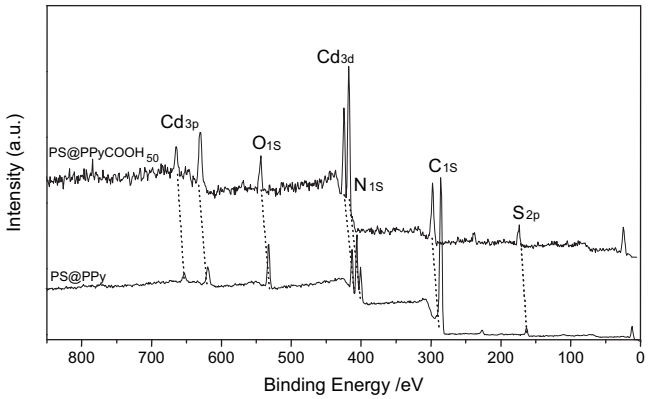


**Fig. 13.** XPS survey scans of CdS-decorated PS@PPy and CdS-decorated PS@PPyCOOH$_{50}$ latex particles at pH 5.

in its oxidized state and positively charged, the electrostatic interaction between PPy-coated PS particles and the positively charged CdS nanoparticles is repulsive. It follows that surface carboxylic acid groups impart a negative charge to PS@PPyCOOH particles which turn to be effective in immobilizing CdS QDs via electrostatic interactions.

On the basis of the published work of Lu and Lin [27], the massively and tightly bound QDs should retain their photoluminescence if it is not boosted-up by polypyrrole as they have shown for electrochemically prepared polypyrrole-CdSe/CdTe nanocomposites films.

PS@PPy and PS@PPyCOOH$_{50}$ were analyzed by XPS after their incubation with the CdS nanoparticles suspension, at pH 5. The survey spectra shown in Fig. 13 display the typical features of the PS@PPy and PS@PPyCOOH$_{50}$ particles (C1s, N1s and O1s) together with relatively intense Cd3d and Cd3p doublets (at 405–412 and 620–650 eV, respectively) from the immobilized CdS nanoparticles. Two new peaks appear also at 162.5 eV and 228 eV, assigned to S2p and S2s energy levels. The S2p position is in line with sulphide species.

### 3.3. Electrochemistry

Electrochemical characterization of the PS@PPyCOOH and PS@PPyCOOH@CdS latex particles was conducted in two different manners: (i) the first consists in the cyclic voltammetry (CV) with latex particles suspended in aqueous solutions of $LiClO_4$ (0.1 M); (ii) the second approach investigates the cyclic voltammetry of latex particle films that have been pre-cast onto ITO working electrodes from aqueous suspensions.

#### 3.3.1. Suspended particles

A glassy carbon disk (4 mm diameter) was used as the working electrode and $LiClO_4$ (0.1 M) was added to the latex suspension, as a supporting electrolyte.

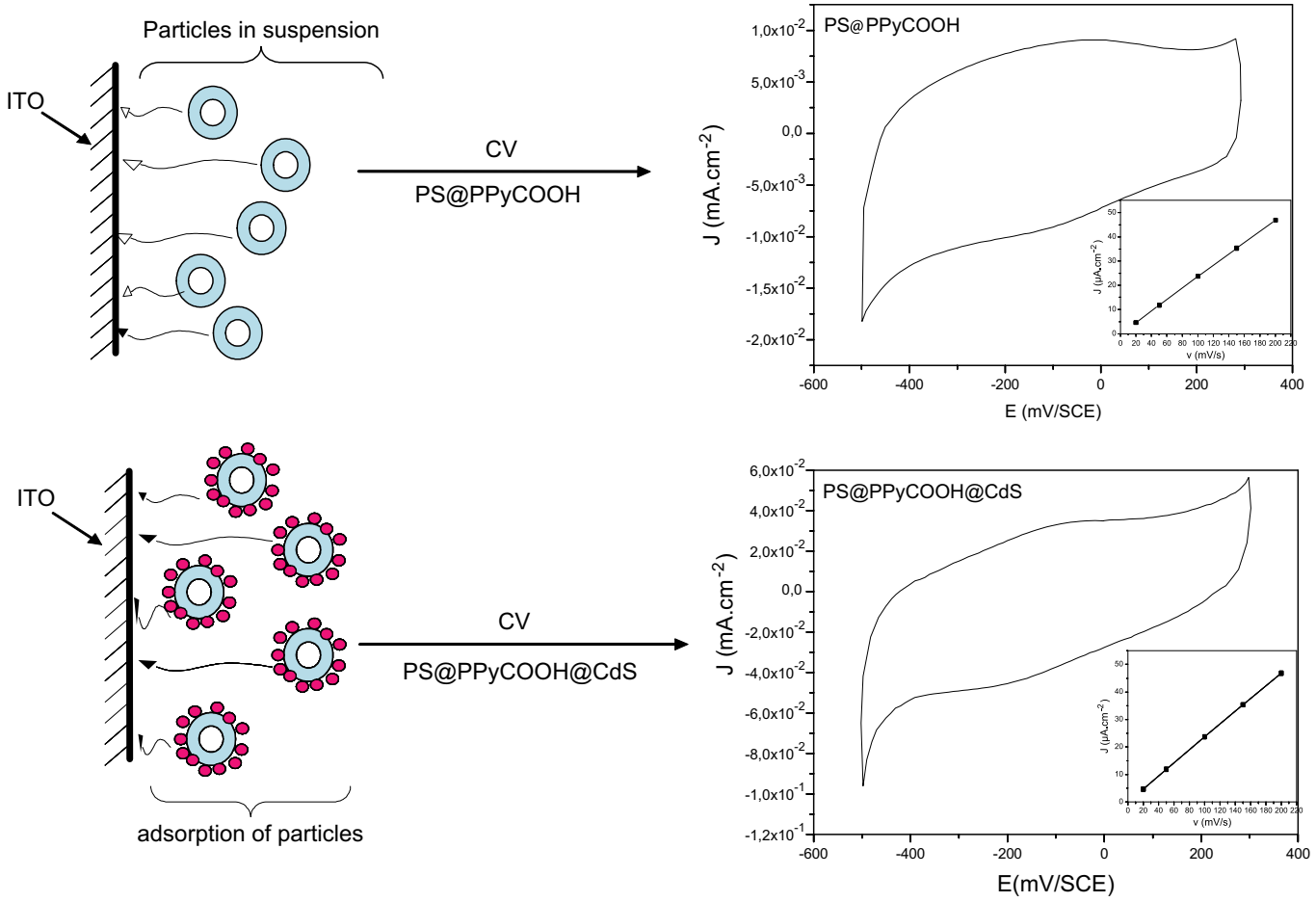


**Fig. 14.** Cyclic voltammograms of the PS@PPyCOOH and PS@PPyCOOH@CdS latex dispersed in 0.1 M LiClO4 (potential scan rate $v = 100$ mV s$^{-1}$). Insets show plots of the anodic peak current $I_a$ versus $v$.

Fig. 14 shows the cyclic voltammograms of PS@PPyCOOH and PS@PPyCOOH@CdS lattices suspended in electrolytic solutions. The latex dispersions were swept through a potential of +0.3 to −0.5 V versus SCE at various scan rates. The CV data indicate that the PS@PPyCOOH and PS@PPyCOOH@CdS particles are electroactive in aqueous medium. However, the electroactivity is rather low, and the anodic and cathodic waves display broad redox peaks. In the insets, the plots of anodic peak current versus the scan rate *v* are linear, which suggests a surface wave by adsorption. Such a behavior is in agreement with previously published results [28] on the redox reactions of polyaniline-coated latex suspensions where digital photographs confirmed the adsorption of the latex particles on the electrode.

### 3.3.2. Particles deposited by evaporation on ITO

50 μl of the latex suspension was gently dropped on an ITO electrode and left to dry. The latex particle-modified ITO plates served as working electrodes.

The electrochemical activity of PS@PPyCOOH and PS@PPyCOOH@CdS assemblies deposited on an ITO electrode was studied in 0.1 M aqueous solution of $LiClO_4$. The assemblies exhibit good electrochemical stability as shown by cyclic voltammetry of the PS@PPyCOOH and PS@PPyCOOH@CdS-coated ITO electrodes (Fig. 15). The voltammogram of PS@PPyCOOH has a couple of broad oxidation and reduction waves at −0.12 and −0.22 V versus SCE, respectively. Such values are in agreement with previously published results on derivatized pyrrole copolymers [29]. As shown in the inset of Fig. 15, the wave currents have linear relationships with potential scan rates in the 20−300 mV/s range, indicating that the mass and electron transfers occur at the electrode surface. One can note the capacitive current obtained with PS@PPyCOOH@CdS-coated ITO and which is higher than that recorded for PS@PPyCOOH assemblies. This is due probably to the particles of CdS immobilized on the carboxylic acid groups. Nevertheless, with the immobilized CdS nanoparticles, the latex particle films can be cycled repeatedly between the conducting (oxidized) and insulating (neutral) state without any sign of degradation.

### 3.3.3. Impedance spectroscopy measurements

Films of PS@PPyCOOH and PS@PPyCOOH@CdS, prepared on indium tin oxide (ITO) electrodes have been analyzed by impedance spectroscopy measurements. The corresponding Nyquist diagrams are represented in Fig. 16. The analysis was conducted with 10 mV ac amplitude at the open circuit potential (OCP), in the frequency range between $10^5$ Hz and 0.1 Hz. The study is carried out in an electrolyte solution $H_2O/LiClO_4$. The curves corresponding to films of PS@PPyCOOH and PS@PPyCOOH@CdS showed a circular part at high frequencies and a linear part at low frequencies that are

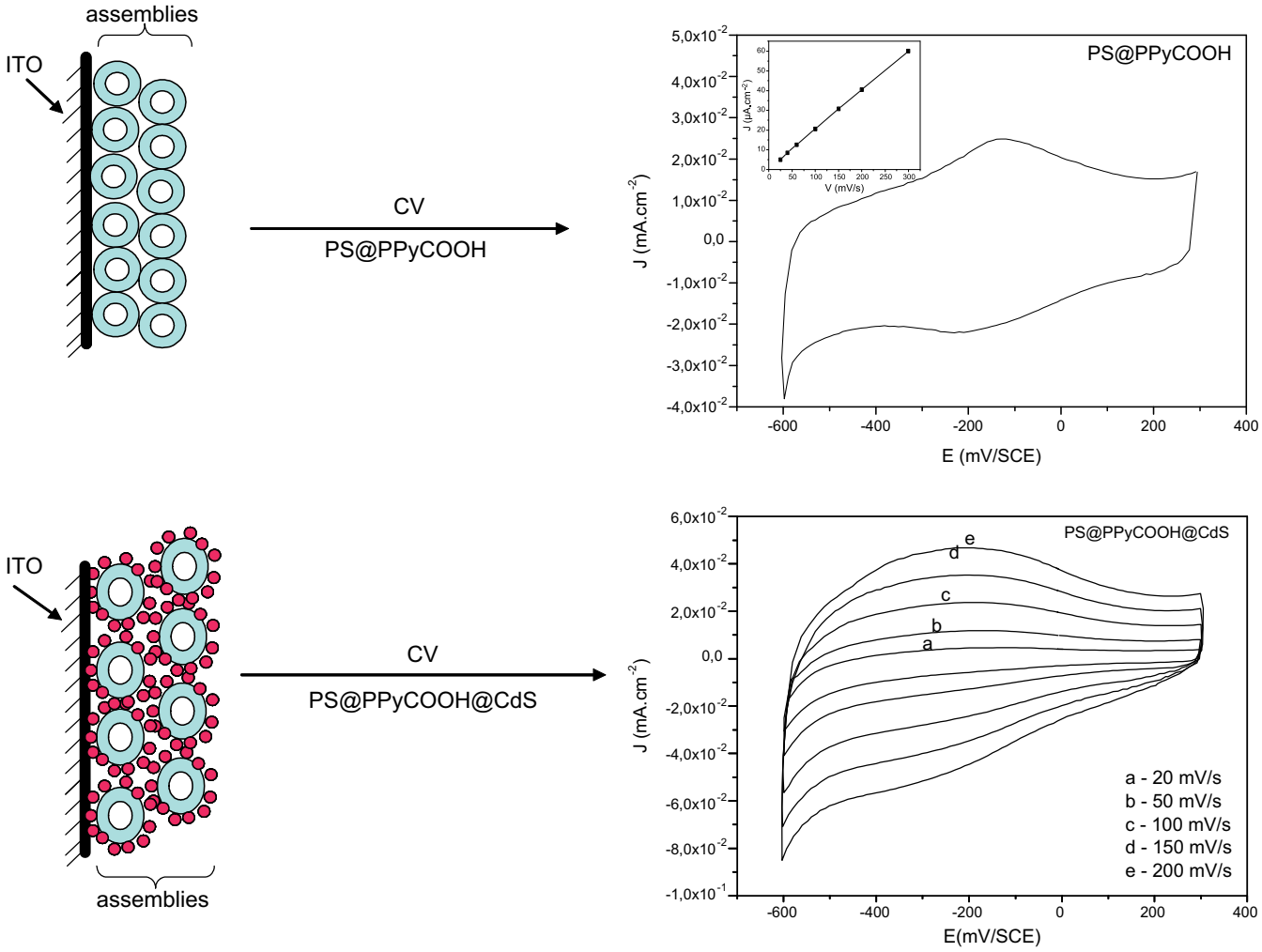


**Fig. 15.** Cyclic voltammograms of the PS@PPyCOOH and PS@PPyCOOH@CdS particle-coated ITO electrodes in aqueous solution containing 0.1 M LiClO4. Insets show plots of the anodic peak current $I_a$ versus *v*.

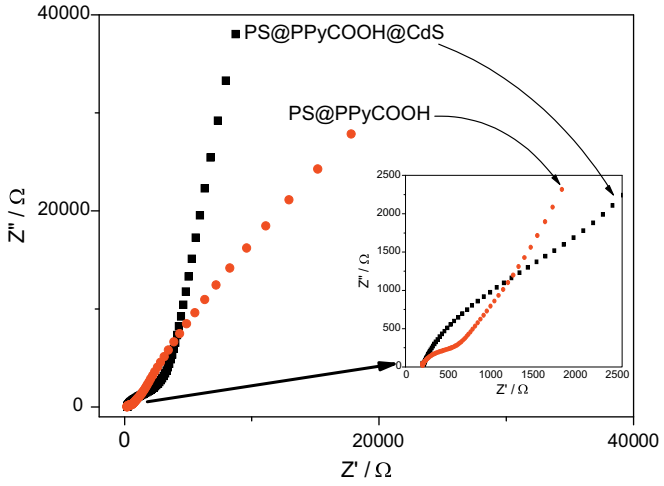


**Fig. 16.** The electrochemical impedance spectroscopy measurements of PS@PPyCOOH and PS@PPyCOOH@CdS.

characteristic of a transfer and diffusion process respectively. In the presence of CdS, the capacitive loop becomes larger and the tangent of the linear part is higher than 1. This indicates that the film becomes more resistant due to the particles of CdS immobilized on the layer of PS@PPyCOOH microspheres. Nevertheless, the CdS-decorated film retains a stable and interesting electrochemical behaviour.

## 4. Conclusion

Polypyrrole-polystyrene latex particles bearing surface *N*-ethyl carboxyl functional groups were prepared in aqueous solution by copolymerization of pyrrole and *N*-carboxylated pyrrole (PyCOOH) using $FeCl_3$ in the presence of PS latexes. The ratio of pyrrole to COOH-functionalized pyrrole monomer was varied and its effect on the surface and the bulk properties of the end products investigated. The PS@PPyCOOH$_x$ particles were characterized in terms of their chemical composition, size, morphology and core–shell structure. TEM showed an increase of the latex particle diameter after coating by the conducting polymer layer, from 390 nm for uncoated PS to 430 nm for PS@PPyCOOH$_{50}$ particles, indicating a PPyCOOH shell thickness of ~20 nm. The core–shell structure of the PS@PPyCOOH$_x$ particles was evidenced by etching the polystyrene core in THF leading to the formation of hollow conducting polymer capsules. We further investigated the self-assembling, via electrostatic interactions, of CdS nanoparticles onto the surface of PS@PPyCOOH$_{50}$ particles. The pH of the reaction medium was found to be an important parameter for the nanoparticles assembly, which could not be obtained when the pH was equal or above 8. In contrast, at pH 5, the carboxylated particles proved to be effective for the electrostatic attachment of CdS nanoparticles, whilst PS@PPy microspheres could not immobilize the quantum dots. The surface carboxylic acid group governs the electrostatic attraction between the positively charged CdS nanoparticles and the PS@PPyCOOH microspheres.

Electrochemical data obtained with PS@PPyCOOH and PS@PPyCOOH@CdS suspensions confirmed that the latex particles are redox-active, with peak currents which are adsorption-limited. The PS@PPyCOOH and PS@PPyCOOH@CdS particles, assembled on ITO electrodes, were also shown to be electroactive with a high stability under potential cycling, particularly for PS@PPyCOOH@CdS.

## Acknowledgements

AM wishes to thank the Algerian Ministry of Higher Education & Scientific Research for financial support. We are indebted to Mrs Carole Connan, Dr Frederic Herbst and Dr Jean-Yves Piquemal (ITODYS, University Paris Diderot) for their efficient assistance with XPS, TEM and TGA studies, respectively.

## References

[1] (a) Maeda S, Armes SP. J Colloid Interface Sci 1993;159:257–9;
(b) Maeda S, Corradi R, Armes SP. Macromolecules 1995;28:2905–11;
(c) Pope MR, Armes SP, Tarcha PJ. Bioconjugate Chem 1996;7:436–44;
(d) McCarthy GP, Armes SP, Greaves SJ, Watts JF. Langmuir 1997;13:3686–92;
(e) Goller MI, Barthet C, McCarthy GP, Corradi R, Newby BP, Wilson SA, et al. Colloid Polym Sci 1998;276:1010–8.
[2] (a) Azioune A, Ben Slimane A, Ait Hamou L, Pleuvy A, Chehimi MM, Perruchot C, et al. Langmuir 2004;20:3350–6;
(b) Azioune A, Pech K, Saoudi B, Chehimi MM, McCarthy G, Armes SP. Synth Met 1999;102:1419–20;
(c) Saoudi B, Jammul N, Chehimi MM, McCarthy GP, Armes SP. J Colloid Interface Sci 1997;192:269–73.
[3] (a) Omastová M, Boukerma K, Chehimi MM, Trchová M. Mater Res Bull 2005;40:749–65;
(b) Boukerma K, Piquemal JY, Chehimi MM, Mravčáková M, Omastová M. Beaunier P. Polymer 2006;47:569–76;
(c) Mravčáková M, Omastová M, Olejníková K, Pukánszky B, Chehimi MM. Synth Met 2007;157:347–57;
(d) Mravčáková M, Boukerma K, Omastová M, Chehimi MM. Mater Sci Eng C 2006;26:306–13;
(e) Mičušik M, Omastová M, Boukerma K, Albouy A, Chehimi MM, Trchová M, et al. Polym Eng Sci 2007;47:1198–206;
(f) Ben Slimane A, Connan C, Vaulay MJ, Chehimi MM. Colloids Surf A Physicochem Eng Asp 2009;332:157–63.
[4] (a) Feng X, Huang H, Ye Q, Zhu JJ, Hou W. J Phys Chem C 2007;111:8463–8;
(b) Pinter E, Patakfalvi R, Fulei T, Gingl Z, Dekany I, Visy CE. J Phys Chem B 2005;109:17474–8;
(c) Han Y, Lu Y. Carbon 2007;45:2394–9;
(d) Ignatova M, Labaye D, Lenoir S, Strivay D, Jérôme R, Jérôme C. Langmuir 2003;19:8971–9;
(e) Zhang X, Lu Z, Wen M, Liang H, Zhang J, Liu Z. J Phys Chem B 2005;109:1101–7;
(g) Perruchot C, Chehimi MM, Delamar M, Dardoize F. J Chrom A 2002;969:167–80.
[5] (a) Yassar A, Roncali J. Garnier F. Polym Commun 1987;28:103–4;
(b) Wiersma AE, Steeg LMA, Jongeling TJM. Synth Met 1995;71:2269–70;
(c) Lascelles SF, Armes SP. J Mater Chem 1997;7:1339–47;
(d) Khan AM, Armes SP. Adv Mater 2000;12:671–4.
[6] (a) Fujii S, Armes SP, Devonshire R, Warren S, McArthur SL, Burchell MJ, et al. Chem Mater 2006;18:2758–65;
(b) Goldsworthy BJ, Burchell MJ, Cole MJ, Armes SP, Khan MA, Lascelles SF, et al. Astronomy Astrophys 2003;409:1151–67;
(c) Burchell MJ, Willisa MJ, Armes SP, Khan MA, Percy MJ, Perruchot C. Planet Space Sci 2002;50:1025–35;
(d) Burchell MJ, Foster NJ, Ormond-Prout J, Dupin D, Armes SP. Meteorit Planet Sci 2009;44:1407–19;
(e) Srama R, Woiwode W, Postberg F, Armes SP, Fujii S, Dupin D, et al. Rapid Commun Mass Spectrom 2009;23:3895–906.
[7] (a) Omastová M, Pionteck J, Kosina S. Eur Polym J 1996;32:681–9;
(b) Omastová M, Kosina S, Pionteck J, Janke A, Pavlinec J. Synt Met 1996;81:49–57;
(c) Ouyang M, Chan CM. Polymer 1998;39:1857–62;
(d) Ben Slimane A, Chehimi MM, Vaulay MJ. Colloid Polym Sci 2004;282:314–23.
[8] (a) Lu Y, Pich A, Adler HJP, Wang G, Rais D, Nešpůrek S. Polymer 2008;49:5002–12;
(b) Adler HJP, Jaehne E, Henke A, Yan L, Pich A. Macromol Symp 2002;187:53–64.
[9] (a) Bousalem S, Yassar A, Basinska T, Miksa B, Slomkowski S, Azioune A, et al. Polym Adv Technol 2003;14:820–5;
(b) Benabderrahmane S, Bousalem S, Mangeney C, Azioune A, Vaulay MJ, Chehimi MM. Polymer 2005;46:1339–46;
(c) Bousalem S, Mangeney C, Alcote Y, Chehimi MM, Basinska T, Slomkowski S. Colloid Surf A Physicochem Eng Asp 2004;249:91–4;
(d) Bousalem S, Mangeney C, Chehimi MM, Basinska T, Miksa B, Slomkowski S. Colloid Polym Sci 2004;282:1301–7;
(e) Bousalem S, Benabderrahmane S, Sang YYC, Mangeney C, Chehimi MM. J Mater Chem 2005;15:3109–16;
(f) Mangeney C, Bousalem S, Connan C, Vaulay MJ, Bernard S, Chehimi MM. Langmuir 2006;22:10163–9;
(g) Mangeney C, Fertani M, Bousalem S, Zhicai M, Ammar S, Herbst F, et al. Langmuir 2007;23:10940–9.

[10] Tlili C, Jaffrezic-Renault N, Martelet C, Korri-Youssoufi H. Mater Sci Eng C 2008;28:848–54.
[11] (a) Chen A, Kamata K, Nakagawa M, Iyoda T, Wang H, Li X. J Phys Chem B 2005;109:18283–8;
(b) Chen A, Wang H, Li X. Chem Commun 2005:1863–4.
[12] Henry MC, Hsueh CC, Timko BP, Freund MS. J Electrochem Soc 2001;148: 155–62.
[13] Stroyuk AL, Kryukov AI, Kuchmii SY, Pokhodenko VD. Theor Exp Chem 2005;41:207–28.
[14] Deng J, Wang L, Liu L, Yang W. Prog Polym Sci 2009;34:156–93.
[15] Travas-Sejdic J, Peng H, Cooney RP, Bowmaker GA, Cannell MB, Soeller C. Curr Appl Phys 2006;6:562–6.
[16] Feldmann C, Metzmacher C. J Mater Chem 2001;11:2603–6.
[17] Al Terary S, Mangeney C, Brayner R, Antoun T, Fiévet F, Yassar A. Sensor Lett 2008;6:511–7.
[18] Antoun T, Brayner R, Al Terary S, Fiévet F, Chehimi MM, Yassar A. Eur J Inorg Chem 2007:1275–84.
[19] Cairns DB, Armes SP, Bremer LGB. Langmuir 1999;15:8052–8.
[20] Lee J-W, Serna F, Nickels J, Schmidt CE. Biomacromolecules 2006;7: 1692–5.
[21] Cairns DB, Khan MA, Perruchot C, Riede A, Armes SP. Chem Mater 2003;15: 233–9.
[22] Lascelles SF, Armes SP. Adv Mater 1995;7:864–6.
[23] Freeman RG, Hommer MB, Grabar KC, Jackson MA, Natan MJ. J Phys Chem 1996;100:718–24.
[24] Perruchot C, Chehimi MM, Delamar M, Lascelles SF, Armes SP. Langmuir 1996;12:3245–51.
[25] Chehimi MM, Azioune A, Bousalem S, Ben Slimane A, Yassar A. In: Elaissari A, editor. Surfactant Sci Ser, vol. 115. New York: Marcel Dekker Inc.; 2003. p. 245–84 [chapter 10].
[26] Tascıoglu S, Tas D. Colloids Surf A 2007;302:349–53.
[27] Lu S-Y, Lin I-H. J Phys Chem B 2003;107:6974–8.
[28] Aoki K, Chen J, Ke Q, Armes SP, Randall DP. Langmuir 2003;19:5511–6.
[29] Korri-Youssoufi H, Makrouf B, Yassar A. Mat Sci Eng C 2001;15:265–8.